

Coordination Chemistry

A Racemic and Enantiopure Unsymmetric Diiron(III) Complex with a Chiral *o*-Carborane-Based Pyridylalcohol Ligand: Combined Chiroptical, Magnetic, and Nonlinear Optical Properties

Florencia Di Salvo,^[a, b] Min Ying Tsang,^[a] Francesc Teixidor,^[a] Clara Viñas,^[a] José Giner Planas,^{*[a]} Jeanne Crassous,^[c] Nicolas Vanthuyne,^[d] Núria Aliaga-Alcalde,^[e] Eliseo Ruiz,^[f] Gerard Coquerel,^[g] Simon Clevers,^[g] Valerie Dupray,^[g] Duane Choquesillo-Lazarte,^[h] Mark E. Light,^[i] and Michael B. Hursthouse^[i, j]

Abstract: The design of molecule-based systems combining magnetic, chiroptical and second-order optical nonlinear properties is still very rare. We report an unusually unsymmetric diiron(III) complex **1**, in which three bulky chiral carboranylpyridinealkoxide ligands (*o*CBhmp⁻) bridge both metal ions and the complex shows the above-mentioned properties. The introduction of *o*-carborane into the 2-(hydroxymethyl)pyridine (hmpH) architecture significantly alters the coordination of the simple or aryl-substituted 2-hmpH. The unusual architecture observed in **1** seems to be trig-

gered by the poor nucleophilicity of our alkoxide ligand (*o*CBhmp⁻). A very rare case of spontaneous resolution takes place on precipitation or exposure to solvent vapor for the bulk compound, as confirmed by a combination of single-crystal and powder X-ray diffraction, second-harmonic generation, and circular dichroism. The corresponding enantiopure complexes (+)**1** and (-)**1** have also been synthesized and fully characterized. This research provides a new building block with unique geometry and electronics to construct coordination complexes with multifunctional properties.

Introduction

The introduction of chirality into coordination compounds has attracted much attention due to their applications in such areas as enantioselective separation, catalysis, nonlinear optics, sensors, and chiral switches.^[1] Of particular interest is the combination of several properties within the same chiral molecule to reveal fascinating effects, such as magnetochirality.^[2] New synthetic strategies to achieve chiral coordination compounds

with unprecedented architectures and combinations of properties are, therefore, in high demand for the development of novel chiral materials. In particular, N,O ligands, such as (hydroxymethyl)pyridines (hmpH; Scheme 1), have proved to be successful building blocks for the self-assembly of metallo-supramolecular architectures with exciting physical properties.^[3] However, only achiral hmpH ligands have been employed in coordination compounds. We have recently described the synthesis and molecular and supramolecular char-

[a] Dr. F. Di Salvo, M. Y. Tsang, Prof. Dr. F. Teixidor, Prof. Dr. C. Viñas, Dr. J. G. Planas
Institut de Ciència de Materials de Barcelona (ICMAB-CSIC)
Campus U.A.B. 08193 Bellaterra (Spain)
E-mail: jginerplanas@icmab.es

[b] Dr. F. Di Salvo
Departamento de Química Inorgánica, Analítica, y Química Física
Facultad de Ciencias Exactas y Naturales, Universidad de Buenos Aires
INQUIMAE-CONICET, Ciudad Universitaria
Pabellón 2, C1428EHA Buenos Aires (Argentina)

[c] Dr. J. Crassous
Institut des Sciences Chimiques de Rennes
Campus de Beaulieu, UMR 6226 CNRS
Université de Rennes 1, 35042 Rennes Cedex (France)

[d] Dr. N. Vanthuyne
Aix Marseille Université, Centrale Marseille, CNRS
iSm2 UMR 7313, 13397 Marseille (France)

[e] Prof. Dr. N. Aliaga-Alcalde
Institució Catalana de Recerca i Estudis Avançats (ICREA)
Institut de Ciència de Materials de Barcelona (ICMAB-CSIC)
Campus de la UAB, 08193 Bellaterra (Spain)

[f] Prof. Dr. E. Ruiz
Departament de Química Inorgànica and
Institut de Recerca de Química Teòrica i Computacional
Universitat de Barcelona, Diagonal 647, 08028 (Spain)

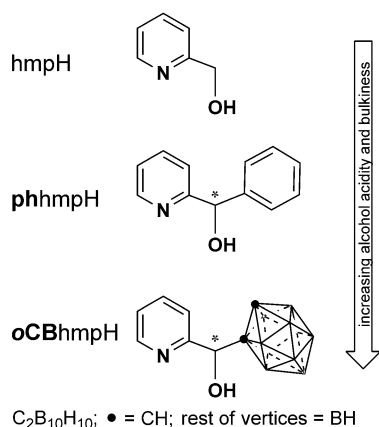
[g] Prof. Dr. G. Coquerel, Dr. S. Clevers, Dr. V. Dupray
Unité de Cristallogénèse, Sciences et Méthodes Séparatives (SMS)
UPRES EA 3233, IRCOF IMR 4114, Université de ROUEN
Rue Tesnière, F-76821 Mont Saint-Aignan Cedex (France)

[h] Dr. D. Choquesillo-Lazarte
Laboratorio de Estudios Cristalográficos
IACT-CSIC, Armilla, Granada (Spain)

[i] Dr. M. E. Light, Prof. Dr. M. B. Hursthouse
School of Chemistry, University of Southampton
Highfield, Southampton. UK SO17 1BJ (UK)

[j] Prof. Dr. M. B. Hursthouse
Department of Chemistry, Faculty of Science
King Abdulaziz University, Jeddah 21588 (Saudi Arabia)

 Supporting information for this article is available on the WWW under <http://dx.doi.org/10.1002/chem.201303037>.



Scheme 1. 2-(Hydroxymethyl)pyridine (hmpH)-related ligands.

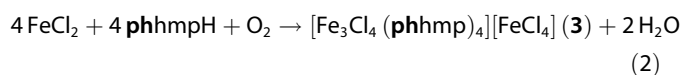
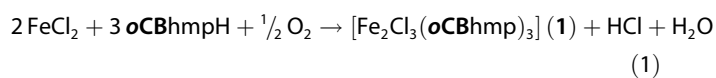
acterization of a series of chiral nitrogenated aromatic carboranyl alcohols, such as (*o*-carboranyl)(2-hydroxymethyl)pyridine (**oCBhmpH**; shown in Scheme 1).^[4] These new compounds, which are prepared in very good yields from one-pot reactions in racemic form, can be regarded as a hmpH ligand in which one of the H atoms at the CH₂ position of the alcohol arm has been replaced by an *o*-carboranyl fragment (*closo*-1,2-C₂B₁₀H₁₁) to give *o*-carboranyl-hmpH (**oCBhmpH**; Scheme 1). The icosahedral *closo* carboranes (dicarba-*closo*-dodecaboranes; C₂B₁₀H₁₂) are an interesting class of exceptionally stable boron-rich clusters that can be modified at different vertices through chemical reactions.^[5] The high thermal and chemical stability, hydrophobicity, acceptor character, and three-dimensional nature of the icosahedral carborane clusters make these new molecules valuable ligands in coordination chemistry. The average size of the *o*-carborane (148 Å³) is comparable to that of adamantane (136 Å³) and is significantly larger (40%) than the phenyl ring rotation envelope (102 Å³).^[6] Regarding the electronic effect, *o*-carborane behaves as a strong electron-withdrawing group (similar to fluorinated aryl) on a substituent at one of the cluster carbons.^[6,7] Thus, introduction of *o*-carborane into the hmpH backbone is expected to exert a higher decrease of the alcohol p*K*_a value with respect to the related phenyl-hmpH (**phhmpH**) derivative (Scheme 1). On the other hand, introduction of *o*-carborane leads to an increase in the size and hydrophobicity of **oCBhmpH** with respect to **phhmpH**. Importantly, the alterations provoked by the introduction of *o*-carborane into hmpH cannot be considered individually because usually a number of properties are influenced simultaneously. For example, we have recently published our first results on the metallosupramolecular chemistry of **oCBhmpH** with cobalt, which gives a rare example of an anti-ferromagnetic complex with porous channels.^[8] The porosity in this complex seems to be triggered by the self-assembly of staggered carborane fragments along hydrogen-bonding networks. It also appears that the chirality in conjunction with the bulky carborane favors *RR/SS* alternation in the supramolecular chains as a more compact packing arrangement.

Following our previous results, the next challenge is to resolve the enantiomers of our ligand or the related metal complexes with the expectation that novel properties would add to those found in the racemic complexes.^[8] Herein, we focus our interest on iron complexes. Although iron is inexpensive, non-toxic, very abundant, and environmental friendly, known chiral enantiopure iron-based molecular materials are very limited.^[9] We now report the synthesis of a dinuclear chiral iron complex, both in racemic and enantiopure forms, with unusual asymmetry triggered by the *o*-carborane-based ligand **oCBhmpH** and compared with the corresponding phenyl-hmpH (**phhmpH**) derivative. Structural, chiroptical, and magnetic properties of the **oCBhmpH** complexes are reported and discussed. Molecular materials that combine magnetic, chiroptical, and second-order optical nonlinear properties are still very rare.^[10]

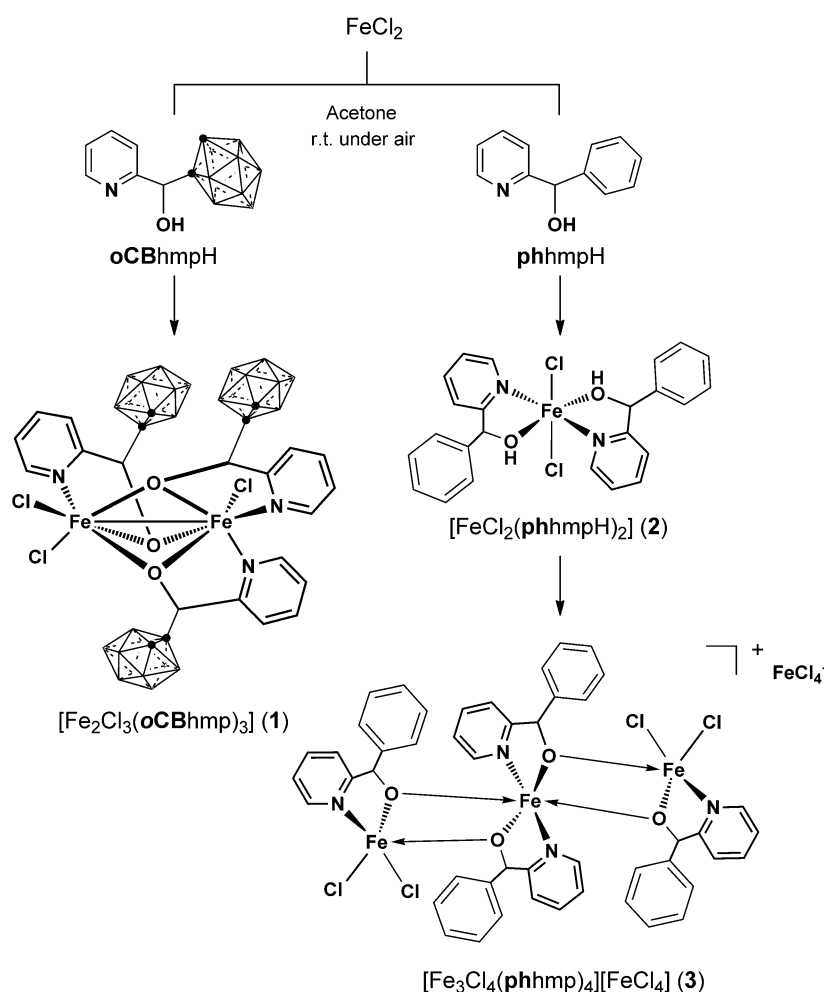
Results and Discussion

The reaction of **oCBhmpH** with FeCl₂ in a 1.5:1 ratio in acetone gave a clear yellowish golden solution from which the Fe^{III} complex [Fe₂Cl₃(**oCBhmpH**)₃] (**1**) was subsequently isolated in nearly quantitative yield (Scheme 2). Small variations in the Fe^{II}/**oCBhmpH** ratio also gave complex **1**. When the same reaction was carried out with the phenyl-modified ligand **phhmpH**, initial formation of the mononuclear Fe^{II} complex [FeCl₂(**phhmpH**)₂] (**2**) was observed, followed by its conversion to the trinuclear Fe^{III} complex [Fe₃Cl₄(**phhmpH**)₄][FeCl₄] (**3**). A comparison of the reactions with **oCB**- and **phhmpH** is shown in Scheme 2.

Clearly, Fe^{III} complexes **1** and **3** are the preferred products of the reactions under these conditions. The stability of complex **3** is further confirmed in a recent report in which its formation was shown by hydrolysis and reduction of the related phenylpyridine-2-yl-methanone oxime ligand in the presence of FeCl₃ under solvothermal conditions.^[11] We have confirmed the structure of **3** by using single-crystal X-ray diffraction (XRD) studies (Figure S11 in the Supporting Information) and the phase purity of the final product by using elemental analysis. The formation of these complexes is summarized in Equations (1) and (2), assuming atmospheric O₂ is the oxidizing agent.



Note that no base is added to abstract the alcohol protons in these two related ligands. However, in the final complexes (**1** and **3**) the ligands are both deprotonated. An increasing tendency to deprotonation of alcohols upon coordination is expected with increasing hardness of the metal ion.^[12] Group 7 and 8 transition metals are in an intermediate situation in which either protonated or deprotonated coordinated alcohols



Scheme 2.

are found. It is in these intermediate situations that the acidity of the alcohols might make a difference. As previously mentioned, our carborane-based ligand **oCBhmpH** is expected to be more acidic than the related **PhhmpH** due to the greater electron-withdrawing character of the *o*-carboranyl than that of the phenyl moiety.^[6,7] This is indirectly confirmed by the isolation and single-crystal XRD studies of the intermediate mononuclear Fe^{II} complex [FeCl₂(**phhmpH**)₂] (**2**), in which the alcohol moieties remain protonated (Figure S13 in the Supporting Information). No such reaction intermediate was observed during the formation of [Fe₂Cl₃(**oCBhmp**)₃] (**1**) even under an N₂ atmosphere by using NMR spectroscopy.

Racemic complex **1** was characterized by using elemental analysis, IR, cyclic voltammetry, and UV/Vis spectrometry. The molecular structure for complex **1** was unequivocally established by single-crystal XRD. Two crystal structures have been determined from racemic [Fe₂Cl₃(**oCBhmp**)₃] (**1**), an acetone solvate [Fe₂Cl₃(**oCBhmp**)₃]·acetone (**1**·acetone; Figure 1) and an ether solvate [Fe₂Cl₃(**oCBhmp**)₃]·ether (**1**·ether; Figure S10 in the Supporting Information). The molecular structure for compound **1** shows a dinuclear Fe^{III} system with rather unusual asymmetry. Both solvated structures of complex **1** show the

same arrangement of ligands and consist of two distorted octahedral metal ions bridged by three **oCBhmp**⁻ ligands, each of which uses its alkoxide functionality to link the two Fe^{III} ions. The remaining pyridine rings on each of the carborane-based ligands are also coordinated in a monodentate fashion, so that the octahedral coordination of one Fe^{III} ion is completed by two pyridine nitrogen atoms and a terminal Cl⁻ ion and the other Fe^{III} is completed by one pyridine nitrogen and two terminal Cl⁻ ions. The **oCBhmp**⁻ ligands thus feature a μ-κ¹O: κ²N,O bonding mode, which leads to a unique unsymmetrical dinuclear Fe^{III} complex with three alkoxide bridges. Due to the unsymmetric nature of complex **1**, the Fe–O bonds show some differences. The average length of the three Fe1–O bonds (2.017 Å) is 0.085 Å shorter than the related Fe2–O bonds (2.102 Å) in structure **1**·acetone. This difference is less pronounced in the ether solvate **1**·ether (0.022 Å). The three Fe–N bonds and three Fe–Cl bonds have similar lengths and are in agreement with values found in other Fe^{III} complexes.

The geometrical constraints imposed by the chelating and bridging coordination modes of the three **oCBhmp**⁻ ligands in **1** (**1**·acetone/**1**·ether mean chelation N–Fe–O angle: 78.1/77.4°, mean O–Fe–O angle: 88.4/88.5°) result in a significant distorted octahedral geometry for both metal centers (with the

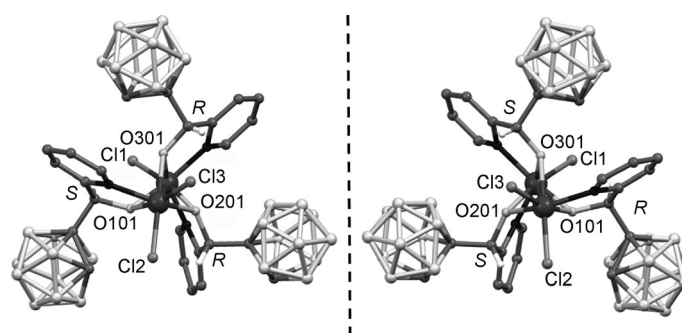
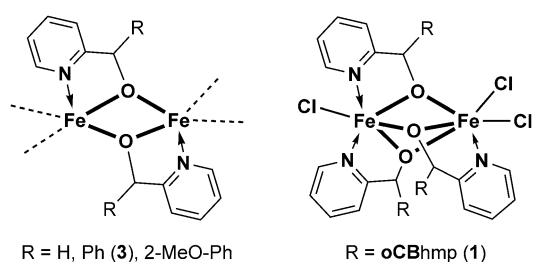


Figure 1. Ball-and-stick representation (Mercury 3.0)^[16] of the molecular structure of **1**·acetone, showing both enantiomers in the racemate. All hydrogen atoms, except those for the CHOH group, are omitted for clarity. Black spheres = N, light grey spheres = B, dark grey spheres = C, larger spheres = Fe, other atoms labeled.

largest deviation of the axial angle from the ideal 180° being for N101-Fe2-O201 at 150.8(3)° and N201-Fe2-O301 at 150.2(1)° in **1**-acetone and **1**-ether, respectively). The Fe–Fe separations of 2.8722(15) Å and 2.8843(8) Å are short enough to be consistent with a bonding interaction between the metals. Fe^{III} complexes with short Fe–Fe contacts have been reported in the literature,^[13] the shortest bond being 2.714 Å.^[14] A search in the CCDC shows only one example of a dinuclear Fe^{III} compound with three citrate bridges but the complex is symmetric.^[15]

The deprotonation of the alcohol functionalities in hmpH and its derivatives is known to favor bridging (μ - κ^1 O: κ^2 N,O) over chelating (N,OH) bonding modes and this is a widely used strategy for fostering formation of polynuclear complexes.^[3b] Introducing substituents of controllable bulk near the alkoxide functional group seems to affect the polynuclearity of the related complexes in the sense of lowering the nuclearity for bulkier substituents and vice versa. This could also explain the formation of a dinuclear Fe^{III} complex in the case of **1** (*o*-carboranyl-substituted) against a trinuclear complex in the case of **3** (phenyl-substituted). However, it is worth noting that regardless of the nuclearity of the iron complexes formed, in all other reported noncarboxylate Fe^{III} complexes in the literature with hmpH or any related derivatives, two alkoxide pyridylalcohol ligands always bridge two close Fe^{III} ions (Scheme 3, left).^[12,17] Or in other words, all reported Fe^{III} complexes with 2-pyridylalcohol ligands contain (in the absence of



Scheme 3. μ_2 -O versus μ_3 -O bridging of hmpH in Fe complexes.^[18]

carboxylate ligands) an even number of alkoxide bridges, regardless of the nuclearity. This is in sharp contrast with dinuclear complex **1**, which has three alkoxide bridges, that is, an odd number of chiral pyridylalcohol ligands (Scheme 3, right). The expected higher acidity of our ligands compared with other hmpH-related ligands makes our alkoxide ligand (**oCBhmp**[−]) less basic and, therefore, less nucleophilic and consequently less coordinating at oxygen.^[18] In such a case, a third alkoxide pyridylalcohol ligand might compensate the electron densities at the metals better. We cannot however rule out the possible role that the bulky carborane fragments might have in the entropy of the reaction. The presence of three alkoxide bridges in **1** is rather surprising owing to the size of the carborane cages and it has important structural consequences. Each of the pyridylalcohol ligands can adopt an *R* or *S* configuration, so that *RRR*, *SSS*, *RRS*, and *SSR* could all be expected in complex **1**. However, only *RRS* and *SSR* combinations are found

in the structure for **1** (Figure 1). Careful examination of the structures for **1** suggests that *RRR* or *SSS* ligand combinations would not fit around a dinuclear Fe^{III} core due to the steric hindrance imposed by the handedness of the ligands. To confirm the latter assumption, the direct stereoselective synthesis of an enantiopure complex **1** from pure *R* and *S* enantiomers of **oCBhmpH** was investigated.

The *R* and *S* enantiomers of **oCBhmpH** were resolved by using HPLC over a chiral stationary phase (see the Supporting Information) and the absolute configurations were determined by using single-crystal XRD (*(R)*-(+)-**oCBhmpH**, *ee* > 95.5%; *(S)*-(-)-**oCBhmpH**, *ee* > 95.5%).^[19] Addition of FeCl₂ to *(R)*-(+)-**oCBhmpH**/*(S)*-(-)-**oCBhmpH** mixtures (1:0.5 equiv or 0.5:1 equiv per 1 equiv of Fe) in acetone quantitatively produced the corresponding enantiopure complexes [Fe₂Cl₂((*RRS*)-**oCBhmp**)₃] ((*RRS*)-(-)-**1**) or [Fe₂Cl₂((*SSR*)-**oCBhmp**)₃] ((*SSR*)-(+)-**1**)^[27] and have been characterized by using IR and XRD (Figures S11 and S12 in the Supporting Information). Both enantiopure metal complexes crystallize in the chiral space group *P*2₁, with Flack parameters of 0.028(7) ((*RRS*)-(-)-**1**) and 0.033(8) ((*SSR*)-(+)-**1**); the latter is isostructural to **1**-ether. When only one of the enantiomers was employed (*(R)*-(+)-**oCBhmpH** or *(S)*-(-)-**oCBhmpH** with FeCl₂ in a 1.5:1 ratio), a mixture of a dinuclear [Fe₂Cl₂((*RR*)-**oCBhmp**)₂]-acetone (**4**-acetone) and mononuclear [Fe((*SSS*)-**oCBhmp**)₃] (**5**) were formed and have been characterized by using XRD (Figure 2) and PXRD (Figure S9 in the Supporting Information). Complexes **4**-acetone and **5** crystallize in the chiral space groups *P*4₁,2

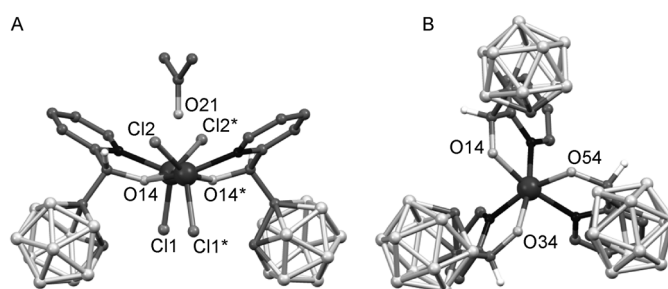


Figure 2. Ball-and-stick representation (Mercury 3.0)^[16] of the molecular structures of A) [Fe₂Cl₂((*RR*)-**oCBhmp**)₂]-acetone (**4**-acetone) and B) [Fe((*SSS*)-**oCBhmp**)₃] (**5**). All hydrogen atoms, except those for the CHO group, are omitted for clarity. Black spheres = N, light grey spheres = B, dark grey spheres = C, larger spheres = Fe, other atoms labeled; * = *x*, *y*, *z*.

(Flack parameter 0.008(4)) and *P*2₁ (Flack parameter 0.009(2)), respectively. Unlike complex **1**, complexes **4** and **5** show symmetrical structures. Whereas in complex **4** two **oCBhmp**[−] ligands with a μ - κ^1 O: κ^2 N,O bonding mode led to a symmetrical dinuclear Fe^{III} complex with two alkoxide bridges, mononuclear complex **5** consists of a *fac*-Fe(**oCBhmp**)₃ molecule in which three **oCBhmp**[−] ligands coordinate through the N and O atoms in a bidentate fashion (Figure 2). It is particularly interesting to compare the X-ray structures for the acetone solvated structures **1**-acetone and **4**-acetone in Figures 1 and 2. The average length of the four Fe–O bonds (2.012 Å) in **4**-acetone is 0.048 Å shorter than the related average length of the six

Fe–O bonds (2.0595 Å) in 1-acetone. However, the Fe–Fe separation in 4-acetone (3.1205(6) Å) is significantly larger (0.248 Å) than the related distance for 1-acetone. Most remarkable is the position of the solvated acetone molecules in both structures. Whereas the acetone molecules are clearly out of the metal coordination spheres in 1-acetone, each acetone molecule in the solid structure for 4-acetone is interacting with the Fe^{III} centers as shown in Figure 2. The acetone interaction mode is unprecedented and can be described as η¹-O coordination of the acetone to the Fe–Fe bond (C=O...Fe_{2,centroid} separation 2.138 Å; angle 180°). It is known that η¹ coordination of ketones to metal centers is preferred over η² for electron-deficient metals.^[20] This data clearly supports our hypothesis that our alkoxide ligand (oCBhmp[−]) is a poor nucleophile and, therefore, a third oxygen, either from an alkoxide pyridylalcohol ligand or a solvent molecule, better compensates the electron densities at the metals. In addition, the data also show that dinuclear complexes with RRR or SSS ligand combinations cannot be formed due to the steric hindrance imposed by the handedness of the oCBhmp[−] ligands.

The circular dichroism (CD) spectra were recorded in solution in CH₂Cl₂ for ligands (R)-(+)-oCBhmpH/(S)-(−)-oCBhmpH and the corresponding metal complexes [Fe₂Cl₃((SSR)-oCBhmp)₃] ((SSR)-(+)·1)/[Fe₂Cl₃((RRS)-oCBhmp)₃] ((RRS)-(−)·1) (Figure 3). In all cases, they display mirror-image values for the (+) and (−) enantiomers within experimental error. Regarding the ligands, their mirror-image CD spectra display structured bands of moderate intensity with Δε values of around −9.3 M^{−1} cm^{−1} at λ = 260 nm for (R)-(+)-oCBhmpH (see dashed lines in Figure 3) that are typical of chiral secondary alcohols with an aromatic substituent.^[20,21] The solution CD spectra for Fe^{III} complexes (RRS)-(−)·1 and (SSR)-(+)·1 are mirror images and display bands at λ = 260, 310, and 350 nm (Δε = −6.4, +1.6, −2.1 M^{−1} cm^{−1}, respectively, for the (RRS)-(−)·1 enantiomer^[20]), which reveals the chiral environment around the iron centers. The CD spectra show that the enantiopure complexes are chemically and configurationally stable in solution. Because the two iron centers show configuration stability, a stereochemical assignment can be proposed for this uncommon chirality around the metal centers by using the A^{Fe} and C^{Fe} stereochemical descriptors to finally give (S,S)-A^{Fe}A^{Fe}-(+)·1 and (R,R)-C^{Fe}-(S)-C^{Fe}-(−)·1 (see the Supporting Information).

As previously mentioned, two crystal structures have been determined for racemic [Fe₂Cl₃(oCBhmp)₃] (*rac*-1), that is, an acetone solvate ([Fe₂Cl₃(oCBhmp)₃·acetone) (1-acetone); Figure 1) and an ether solvate ([Fe₂Cl₃(oCBhmp)₃·ether) (1-ether); Figure S10 in the Supporting Information). The structural analysis of the two solvated

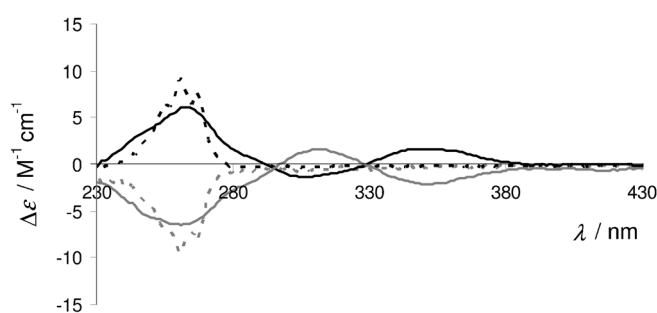


Figure 3. CD spectra of (R)-(+)-oCBhmpH (----), (S)-(−)-oCBhmpH (-----), (R,R)-C^{Fe}-(S)-C^{Fe}-(−)·1 (—), and (S,S)-A^{Fe}-(R)-A^{Fe}-(+)·1 (—).^[20]

structures for 1 revealed that whereas 1-acetone (centrosymmetric *P*₂₁/*c* space group) is a racemate and, therefore, contains both enantiomers ((*RR*)-Fe:(*S*)-Fe and (*SS*)-Fe:(*S*)-Fe; Figure 1), 1-ether is formed by only one of these enantiomers and crystallizes in the non-centrosymmetric and chiral space group *P*₂₁ ((*SS*)-Fe:(*S*)-Fe, Flack parameter 0.004(15)).^[22] Therefore, the latter is the result of spontaneous resolution and conglomerate formation on crystallization (i.e., a physical mixture of enantiomorphous (*RR*)-Fe:(*S*)-Fe and (*SS*)-Fe:(*R*)-Fe crystals).^[23] Because the loss of centrosymmetry is at the origin of the appearance of numerous interesting optical and electrical properties,^[24] we further explored whether total spontaneous resolution or conglomerate formation was possible in entire crystalline batches (i.e., bulk solids). Thus, a crystalline powder obtained by slow evaporation of solutions of 1 in acetone during the workup of the reaction (Figure 4A) could be identified from comparisons of XRPD patterns as a racemic compound (*rac*-1) with the *P*₂₁/*c* space group, isomorphous to 1-acetone (Figure 4B). However, when diethyl ether was added to a solution of *rac*-1 in acetone, a new phase immediately precipitated (virtually no material remained in solution) and was subsequently identified as a conglomerate-forming monoclinic *P*₂₁ form (*co*-1) that was isomorphous to 1-ether (Figure S10 in the Supporting Information). To our knowledge, this is the first switch from a racemic

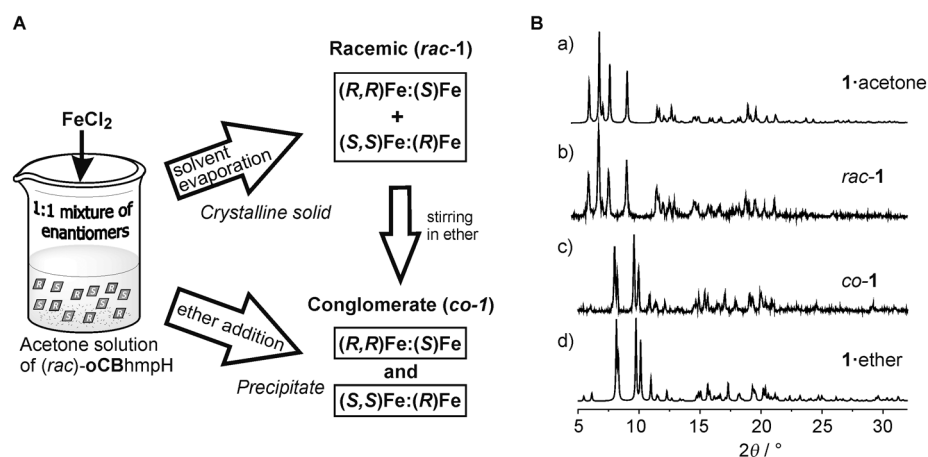


Figure 4. A) Schematic representation of racemic (*rac*-1) and conglomerate (*co*-1) formation for bulk samples of 1, see the text for details. B) XRPD of 1: a) calculated XRPD obtained from the crystal structure of 1-acetone, b) racemic mixture *rac*-1, c) conglomerate *co*-1, d) calculated XRPD obtained from the crystal structure of 1-ether.

compound solvate to a conglomerate solvate on precipitation.^[25] These unexpected results encouraged us to study the possibility of solvent-mediated conglomerate formation in the solid state. The ability of *rac*-1 to take up solvent vapor and convert into *co*-1 has been demonstrated experimentally. Freshly made dried powdered *rac*-1 converts to conglomerate *co*-1 when left in contact with diethyl ether vapor for 3 d (Figure S8 in the Supporting Information). The identity of the products was confirmed by using XRPD, which matched the calculated diffraction patterns from the single-crystal X-ray structures. Thus, the transition from a racemic compound to a conglomerate either on precipitation or exposition to solvent vapor is of particular interest because it corresponds to a spontaneous resolution. We are further investigating the conglomerate formation mechanism.

To confirm the chiral nature of conglomerate solid phase *co*-1, its nonlinear optical activity has been measured by using second-harmonic generation (SHG) measurements. The SHG method is currently used to prescreen conglomerates.^[26] Complex *co*-1 shows a clear positive SHG signal (about 25% quartz; Figure 5) that is consistent with the structure of 1-ether crystallized in the non-centrosymmetric and chiral space group $P2_1$ (see Figure S8 in the Supporting Information). Complex *co*-1 exhibits a relatively poor damage threshold under laser irradiation and remains stable up to 110 °C. The decay of the time-resolved second-harmonic generation (TR-SHG) curve between 110 °C and the decomposition temperature of the complex (≈ 200 °C) could be due to the thermal expansion of the crystal lattice and/or degradation of the sample. Consistent with solid-phase *co*-1 being a conglomerate, that is, a 1:1 mixture of enantiomorphous crystals, the CD spectrum in solution shows no signal.

Solid-state, variable-temperature (2–300 K) magnetic susceptibility data under applied external magnetic fields of 0.03 and 0.5 T were collected for polycrystalline samples of compound 1. The data shows behavior characteristic of an antiferromagnetic species, in which $\chi_M T$ values decrease on lowering

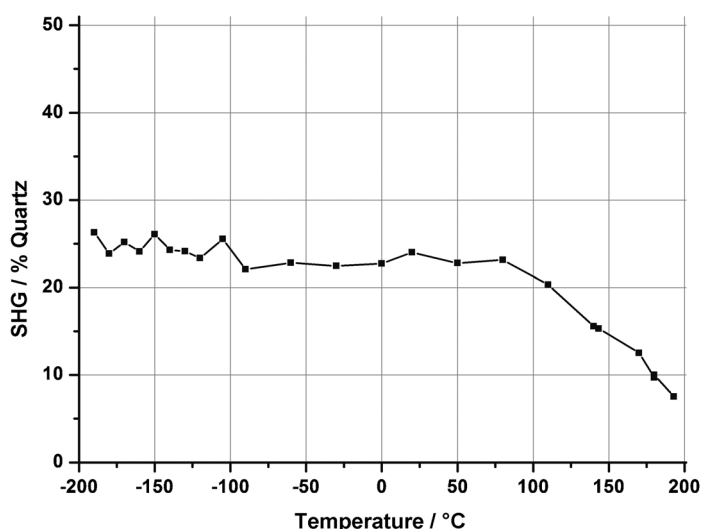


Figure 5. SHG intensity of *co*-1 versus temperature between –200 and 200 °C.

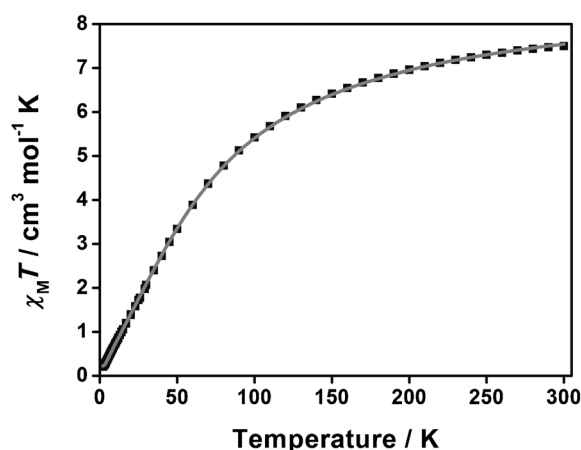


Figure 6. Fitting of the $\chi_M T$ versus T of *rac*-1 between 2 and 300 K. The experimental data are shown as ■ and — corresponds to the fitting values.

the temperature and give a value of $7.50 \text{ cm}^3 \text{mol}^{-1} \text{K}$ at 300 K (Figure 6). This is lower than expected for two independent high-spin Fe^{III} centers of $8.75 \text{ cm}^3 \text{mol}^{-1} \text{K}$ with a g value of 2.00, and is evidence of a significant antiferromagnetic interaction. The graph shows a decrease in the magnetic susceptibility to nearly zero at 2 K ($0.21 \text{ cm}^3 \text{mol}^{-1} \text{K}$). Magnetic susceptibility data were analyzed by using the Van Vleck equation derived from the spin-exchange Hamiltonian $H = -JS_1S_2$,^[27] in which $S_1 = S_2 = 5/2$. The best fit matches well with experimental data and gives values of $g = 2.05$, $J = (-10.22 \pm 0.03) \text{ cm}^{-1}$, $TIP = 280 \times 10^{-6} \text{ cm}^3 \text{mol}^{-1}$, $\rho = 0.05\%$, and $R = 1 \times 10^{-5}$ (see Experimental Section). Overall, the analysis of the data agrees with the shape and values observed in the experimental measurement, in which the exchange coupling for both Fe^{III} atoms is significantly antiferromagnetic. The present data confirm compound 1 as the first dinuclear Fe^{III} system that contains three alkoxide bridges and displays antiferromagnetic behavior. DFT calculations by using B3LYP functional are in agreement with the experimental data, giving a calculated J value of -6.0 cm^{-1} . The analysis of the calculated J values for other complexes with similar bridging ligands corroborates the idea that the Fe–O separation could be the main parameter that controls the magnetic behavior and the longest Fe–O separation of 1 gives an understanding of the antiferromagnetic coupling (see the Supporting Information).

Conclusion

We report an unusually unsymmetric diiron(III) complex 1 in which three bulky chiral carboranylpyridinealkoxide ligands (oCBhmp^-) bridge both metal ions; this complex combines magnetic, chiroptical, and second-order optical nonlinear properties. Complex 1 constitutes the first dinuclear Fe^{III} system that contains three alkoxide bridges and displays antiferromagnetic behavior. DFT calculations have corroborated this behavior and show that the Fe–O separation is the main parameter that controls the magnet-

ic behavior. We showed that the introduction of the bulky *o*-carborane into the 2-(hydroxymethyl)pyridine (hmpH) architecture significantly alters the coordination of the simple or aryl-substituted 2-hmpH. Whereas all other examples in the literature always show two alkoxide pyridylalcohol ligands bridging two close Fe^{III} ions, our dinuclear complex **1** contains three alkoxide bridges. This unusual architecture seems to be triggered by the poor nucleophilicity of our alkoxide ligand (**oCBhmp**⁻). The presence of an odd number of ligands per molecule in **1** results in a reduction of possible enantiomers with the consequent simplicity of the enantiomeric mixture. A very rare case of spontaneous resolution takes place on precipitation or exposure to solvent vapor for the bulk compound, as confirmed by a combination of XRD, XRPD, SHG, and CD measurements. The corresponding enantiopure complexes (+)-**1** and (-)-**1** have also been synthesized and fully characterized. This case study highlights the potential of combining carboranes, coordination chemistry, and chirality in conceiving new molecular materials with unprecedented properties and opens new perspectives in chiral materials.

Experimental Section

Materials

All manipulations were carried out in air unless otherwise noted. The reactions were carried out in glass vials equipped with a magnetic stirring bar and capped with a septum. The following chemicals were used: ethanol (distilled from CaH₂), acetone (distilled from P₂O₅), anhydrous FeCl₂ (98%, Sigma Aldrich; used as received). (2-Pyridine)(*o*-carboranyl)methanol (**oCBhmpH**)^[4b] and (2-pyridine)(phenyl)methanol (**phhmpH**)^[28] were synthesized as previously reported.

General procedure for the synthesis of [Fe₂Cl₃(**oCBhmp**)₃] (**1**) and conglomerate formation

A solution of **oCBhmpH** (75.0 mg, 0.298 mmol) in acetone (0.50 mL) was added to a stirred suspension of FeCl₂ (16.9 mg, 0.131 mmol) in acetone (0.25 mL) in a small capped vial. The vial was closed and the orange-brown mixture was then gently warmed at about 50 °C and shaken until formation of a clear yellowish golden solution. Once the solution was at RT, it was filtered through a Celite leach and left with the cap slightly open. Evaporation of the acetone gave yellow-brown crystalline agglomerates that were dried under vacuum to give *rac*-**1** (71 mg, ≈100%; phase purity established by XRPD, FTIR (ATR), and elemental analysis). Elemental analysis calcd (%) for C₂₈H₅₈B₃₀Cl₃Fe₂N₃O₄·1.5 acetone (1056.15): C 32.41, H 5.44, N 3.09; found: C 32.14, H 5.48, N 3.89.

Transformation of *rac*-**1** into *co*-**1** by precipitation

Addition of diethyl ether (2.0 mL) to a solution of the above *rac*-**1** in acetone gave a suspension that was stirred for 3 h. The supernatant solution was decanted to give a fine pale yellow powder that was dried under vacuum to give ether solvate *co*-**1** (yield: 50 mg, 73%). Phase purity was checked by XRPD, FTIR (ATR), and elemental analysis. M.p. 231 °C (decomp.); elemental analysis calcd (%) for C₂₈H₅₈B₃₀Cl₃Fe₂N₃O₄ (1043.16): C 32.24, H 5.60, N 4.03; found: C 32.25, H 5.65, N 4.01.

Transformation of *rac*-**1** into *co*-**1** by exposure to solvent vapor

A dry polycrystalline sample of complex *rac*-**1** (50 mg) was exposed to vapor of diethyl ether for 3 d. The quantitative formation of *co*-**1** was assessed by comparing the X-ray powder diffraction pattern of the crystalline product with the spectrum calculated on the basis of the single-crystal structure (Figure S8 in the Supporting Information).

In situ NMR spectroscopy studies for formation of **1**

The reaction was performed under inert atmosphere conditions. A solution of **oCBhmpH** (15.5 mg, 0.062 mmol) in degassed [D₃]-acetonitrile (0.50 mL) was added to a NMR tube containing FeCl₂ (5.2 mg, 0.041 mmol), with the tube kept in liquid nitrogen to avoid the reaction starting before measurement. The iced sample was then taken to an NMR spectrometer and ¹H and ¹¹B NMR spectra were recorded. Sharp signals observed for the free ligand became very broad and paramagnetically shifted as soon as the [D₃]-acetonitrile solution melted, which indicated the fast formation of a Fe^{III} compound.

Synthesis of [Fe₂Cl₃((*RRS*)-**oCBhmp**)₃] ((*RRS*)-(-)-**1**)

The general procedure was followed by using (*R*)-(+)-**oCBhmpH** (20.3 mg, 0.081 mmol), (*S*)-(-)-**oCBhmpH** (10.3 mg, 0.041 mmol), and FeCl₂ (10.3 mg, 0.081 mmol). Slow evaporation of the solvent gave complex (*RRS*)-**1** (39.9 mg, 96%) as brown-yellow needles suitable for single-crystal X-ray structure determination. [α]_D²³ = -35.5, [α]₅₇₈²³ = -40.0, [α]₅₄₆²³ = -48.9, [α]₄₃₆²³ = -160 (±5%; CH₂Cl₂, c = 0.24 g/100 mL); UV/Vis: λ = 254 (23 800), 320 (10 200), 356 nm (8000 M⁻¹ cm⁻¹); CD (CH₂Cl₂, C = 2.3 × 10⁻³ M): λ = 260 (-6.4), 310 (+1.6), 350 nm (-2.1 M⁻¹ cm⁻¹).

Synthesis of [Fe₂Cl₃((*RRS*)-**oCBhmp**)₃] ((*SSR*)-(+)-**1**)

The general procedure was followed by using (*S*)-(-)-**oCBhmpH** (20.1 mg, 0.080 mmol), (*S*)-(+)-**oCBhmpH** (10 mg, 0.040 mmol), and FeCl₂ (10.1 mg, 0.080 mmol). Slow evaporation of the solvent gave complex (*RRS*)-**1**·acetone (52.0 mg, 125%) as brown-yellow needles suitable for single-crystal X-ray structure determination. [α]_D²³ = +34.8, [α]₅₇₈²³ = +39.1, [α]₅₄₆²³ = +47.8, [α]₄₃₆²³ = +169.6 (±5%) (CH₂Cl₂, c = 0.23 g/100 mL); UV/Vis: λ = 254 (22 700), 320 (10 000), 356 nm (8000 M⁻¹ cm⁻¹); CD (CH₂Cl₂, C = 2.2 × 10⁻³ M): λ = 260 (+6.0), 310 (-1.3), 350 nm (+1.6 M⁻¹ cm⁻¹).

Synthesis of [FeCl₂(**phhmpH**)₂] (**2**)

A degassed solution of **phhmpH** (20.0 mg, 0.108 mmol) in acetone (0.30 mL) was added to a stirred degassed suspension of anhydrous FeCl₂ (7.0 mg, 0.054 mmol) in acetone (0.25 mL) in a small vial capped with a septum and equipped with a magnetic bar. The mixture was then gently warmed at about 50 °C and stirred until a clear red-yellow solution formed. Once the solution was at RT, the solvent was partially evaporated under a nitrogen gas flow. After 24–36 h, prismatic red crystals were obtained. The identity of the compound was then established by using single-crystal X-ray diffraction. Due to the high solubility and certain instability of the compound, other characterization techniques were not performed. This compound is under further investigations.

Synthesis of $[\text{Fe}_3\text{Cl}_4(\text{phhmp})_4][\text{FeCl}_4]$ (**3**)

The general procedure was followed by using **phhmpH** (30 mg, 0.162 mmol) and FeCl_2 (20.95 mg, 0.162 mmol). Under inert conditions, the red crystalline material from $[\text{FeCl}_2(\text{phhmpH})_2]$ (**2**) formed after 24–36 h, then slowly redissolved to give a yellow solution. Evaporation of the acetone gave yellow crystalline agglomerates that were dried under vacuum to afford **3**. The same procedure under air directly gave compound **3** (42.6 mg, 85%). Purity was established by elemental analysis. Elemental analysis calcd (%) for $\text{C}_{48}\text{H}_{40}\text{Cl}_8\text{Fe}_4\text{N}_4\text{O}_4$ (1243.86): C 46.35, H 3.24, N 4.050; found: C 46.3, H 3.4, N 4.3.

Reaction of FeCl_2 with (*R*)-(+)-**oCBhmpH** or (*S*)-(–)-**oCBhmpH**

The general procedure was followed by using FeCl_2 (10.1 mg, 0.079 mmol) and (*R*)-(+)-**oCBhmpH** (29.5 mg, 0.117 mmol) or FeCl_2 (9.7 mg, 0.077 mmol) and (*S*)-(–)-**oCBhmpH** (30.0 mg, 0.119 mmol). Slow evaporation of the solvent gave mixtures of single crystals and polycrystalline solids that corresponded to **4** and **5**, as determined by XRD (Figure 2) and PXRD (Figure S9 in the Supporting Information).

Physical measurements

Elemental analysis: Elemental analyses (C, H, N) were performed by the Analysis Service of the Universitat Autònoma de Barcelona by using a Carlo Erba CHNS EA-1108 microanalyzer.

FT-IR spectra: FTIR-ATR spectra were recorded by using a Perkin-Elmer 1720X spectrometer.

NMR spectra: ^1H , ^{11}B NMR spectra were recorded at 300 and 96 MHz, respectively, by using a Bruker ARX 300 MHz spectrometer and referenced to the solvent (^1H , residual $[\text{D}_5]\text{acetone}$) or $\text{BF}_3\cdot\text{OEt}_2$ (^{11}B). Chemical shifts (δ) are reported in ppm and coupling constants (J) in Hz.

UV/Vis spectra: UV/Vis measurements were carried out by using a Hewlett Packard 8453 diode array spectrometer equipped with a Lauda RE 207 thermostat and a screw-capped quartz cuvette.

Circular dichroism: Circular dichroism (in $\text{m}^{-1}\text{cm}^{-1}$) and UV/Vis were measured by using a Jasco J-815 Circular Dichroism Spectrometer (IFR140 facility, Université de Rennes 1). Specific rotations were measured in a 1 dm thermostated quartz cell by using a Perkin-Elmer-341 polarimeter.

Cyclic voltammetry: Cyclic voltammetry measurements were made in 0.1 M tetrabutylammonium hexafluorophosphate (TBAF_6) electrolyte solutions in acetonitrile. A two-compartment cell equipped with a glassy carbon working electrode, a platinum gauze as the counter electrode, and an Ag wire as the pseudo-reference electrode, properly checked against a ferrocene/ferrocenium (Fc/Fc^+) couple before test, was used. Measurements were made by using a BASi C-3 Cell Stand. Data were obtained at a scan rate of 100 mV s^{-1} .

X-ray powder diffraction (XRPD): XRPD data was collected by using a Siemens Analytical X-ray D-5000 diffractometer with a $\text{Cu}_{\text{K}\alpha}$ radiation. All XRPD measurements were carried out at RT.

X-ray diffraction studies: Single-crystal intensity data for **1**-acetone was collected at 120 K by using a Bruker Nonius Kappa CCD area detector mounted at the window of a rotating Mo anode ($\lambda(\text{Mo}_{\text{K}\alpha})=0.71073\text{ \AA}$; see Table S1 in the Supporting Information). Data collection and processing were performed by using the programs COLLECT^[29] and DENZO^[30] and a multi-scan absorption correction was applied by using SADABS.^[31] Data for **1**-ether was collected at 100 K by using a Rigaku AFC₁₂ goniometer equipped with

an enhanced sensitivity (HG) Saturn724+ detector mounted at the window of an FR-E+ SuperBright molybdenum rotating anode generator ($\lambda(\text{Mo}_{\text{K}\alpha})=0.71073\text{ \AA}$) with HF Varimax optics (100 μm focus). Data collection and processing, including a multi-scan absorption correction, was performed by using CrystalClear.^[32] The structures were solved by using direct methods^[33] and refined by using full matrix least squares^[34] on F^2 . X-ray reflections for **2** and **3** were collected at 298 K by using an Oxford Xcalibur Gemini Eos CCD diffractometer with $\text{Mo}_{\text{K}\alpha}$ radiation ($\lambda=0.7107\text{ \AA}$; see Table S3 in the Supporting Information). Data collection and processing, including a multi-scan absorption correction, were performed by using CrysAlisPro (v. 1.171.34.55)^[35] and OLEX2-1.2^[36] and SHELXL97^[37] were used for structure solution and refinement. For these structures, several H atoms (especially OH) were detected at approximate locations in a difference Fourier map and then refined freely. Those for BH and some CH were placed in idealized positions and refined by using a riding model, with $\text{C-H}=0.93\text{ \AA}$ and $U_{\text{iso}}(\text{H})=1.2 U_{\text{eq}}(\text{C})$. Data for **4**, **5**, (*RRS*)-**1**, and (*SSR*)-**1** were collected by using a Bruker D8 Venture (**4** and **5**, 150 K, $\lambda=1.54178\text{ \AA}$) or a Bruker SMART APEX diffractometer ((*RRS*)-**1** and (*SSR*)-**1**, 100 K, $\lambda=0.71073\text{ \AA}$). Data collection and processing were performed by using the programs APEX2^[38] and SAINT^[39] and a numerical absorption correction was applied based on indexed crystal faces by using the Crystal Faces plugin in APEX2.^[39] The structures were solved by direct methods,^[34] which revealed the position of all non-hydrogen atoms. These atoms were refined on F^2 by a full-matrix least-squares procedure by using anisotropic displacement parameters.^[34]

Special details: For **1**-acetone, **1**-ether, **2**, **3**, **4**, and **5**, all hydrogen atoms were placed in idealized positions and refined by using a riding model. For (*RRS*)-**1** and (*SSR*)-**1**, the solvent masking procedure as implemented in Olex2^[23] was used to remove the electronic contribution of solvent molecules from the refinement. Each void is postulated to contain ≈ 1.6 ((*RRS*)-**1**) or 1.3 ((*SSR*)-**1**) molecules of acetone.

One of the refined phenyl rings in **3** was modeled as split over two positions (59, 41) and geometric and thermal parameter restraints were applied. During the refinement of complex **3**, residual electron density was detected in the lattice associated with solvent molecules. Thus, the data was treated with the SQUEEZE procedure (from PLATON).^[40] The volume occupied by the solvent was 1257.4 \AA^3 and the number of electrons per unit cell deduced by SQUEEZE was 132, these values were not interpretable as a definitive number of specific solvent molecules.

Second-harmonic generation (SHG): The experimental setup used for the TR-SHG measurements was previously published.^[41] A Nd/YAG Q-switched laser (Quantel) operating at 1.06 μm was used to deliver 360 mJ pulses of 5 ns duration with a repetition rate of 10 Hz. An energy adjustment device made up of two polarizers (P) and a half-wave plate ($k/2$) allowed the incident energy to vary from 0 to $\approx 200\text{ mJ}$ per pulse. A RG1000 filter was used after the energy adjustment device to remove light from laser flash lamps. The samples (a few mg of powder in a crucible) were placed in a computer-controlled heating-cooling stage (Linkam THMS-600) and were irradiated with a beam (diameter 4 mm). The signal generated by the sample (diffused light) was collected by an optical fiber (500 μm core diameter) and directed onto the entrance slit of a spectrometer (Ocean Optics). A boxcar integrator allowed an average spectrum (spectral range $\lambda=490\text{--}590\text{ nm}$) with a resolution of 0.1 nm to be recorded over 2 s (20 pulses). To avoid problems related to the sublimation of the samples, the heating stage was opened but only during the SHG measurements so it had no significant influence on the temperature regulation. According to the

SHG powder method described by Kurtz and Perry,^[42] SHG signal intensities were compared to the signal of a reference compound (quartz; 45 lm average size).

Magnetic measurements: Magnetic measurements were carried out at the Unitat de Mesures Magnètiques (Universitat de Barcelona) on polycrystalline samples by using a Quantum Design SQUID MPMS-XL magnetometer working in the 2–300 K range. The magnetic fields used in the measurements were 0.03 T (from 2–30 K) and 0.5 T (from 2–300 K). Diamagnetic corrections were evaluated from Pascal's constants. The fit was performed by minimizing the function R (agreement factor defined as $\sum[(\chi_m T)^{\text{exptl}} - (\chi_m T)^{\text{calcd}}]^2 / \sum[(\chi_m T)^{\text{exptl}}]^2$) TIP and ρ are defined as temperature-independent parameter and impurities, respectively.

Theoretical calculations: Density functional theory methods provide an excellent estimation of the exchange coupling constants by taking into account the very small energy differences computed to extract the exchange coupling constants.^[43] Because a detailed description of the computational strategy used to calculate the exchange coupling constants in dinuclear and polynuclear complexes is outside the scope of this paper, we will focus our discussion here to its most relevant aspects and a more detailed description can be found elsewhere.^[44–47] For the calculation of the n different coupling constants J_{ij} present in a polynuclear complex, we need to carry out calculations for at least $n+1$ different spin distributions. Thus, by solving the system of n equations obtained from the energy differences we can obtain n coupling constants. For systems in which more than n spin distributions were calculated, a least-square fitting procedure to obtain the coupling constants must be used. In the specific case of dinuclear Fe^{III} complexes, the J value is directly obtained from the energy difference between the high-spin state (parallel alignment of the local spins) and the single-determinant low-spin solution (antiparallel alignment of the local spins), usually called broken symmetry, divided by a $2S_1S_2 + S_1$ term ($S_1 = 5/2$, $S_2 = 5/2$). For the studied symmetric trinuclear Fe_3^{III} complex with two different J values (the second one between the two terminal Fe^{III} centers), three spin configurations have been calculated, that is, the high-spin one and two $S = 5/2$ that correspond to the spin inversion of the central and terminal Fe^{III} cations, respectively. In previous studies,^[4] we found that the hybrid B3LYP functional^[48] together with the basis sets proposed by Schaefer et al.^[49] provide J values in excellent agreement with the experimental ones. We have employed a basis set of triple- ζ quality as proposed by Schaefer et al. The calculations were performed with the Gaussian 09 code^[50] using guess functions generated by using the Jaguar 7.5 code.^[51,52]

Acknowledgements

We thank CICYT (F.D.S., M.Y.T., F.T., C.V., and J.G.P.: grant CTQ2010-16237; N.A.-A. and E.R.: grant CTQ2012-32247; E.R.: grant CTQ2011-23862-C02-01), Generalitat de Catalunya (F.D.S., M.Y.T., F.T., C.V., and J.G.P.: 2009/SGR/00279; E.R.: 2009SGR-1459) and the CSIC (JAE-doc contract to F.D.S.) for financial support. F.D.S. thanks CONICET for support. M.E.L. and M.B.H. thank the UK Engineering and Physical Science Research Council for support by the X-ray facilities at Southampton. M.B.H. thanks the Leverhulme Trust for the award of an Emeritus Fellowship. M.Y.T. is enrolled in the UAB PhD program. The project "Factoría de Cristalización, CONSOLIDER INGENIO-2010" provided X-ray structural facilities for this work. E.R. gratefully acknowledges the computer resources, technical expertise, and

assistance provided by the CESCO. J.C. acknowledges the CNRS, the University of Rennes 1, and the ANR (12-BS07-0004-METALHEL-01). Michel Gruselle and Jamal Moussa are warmly thanked for fruitful discussions on stereochemical aspects.

Keywords: boron • chirality • iron • second-harmonic generation • spontaneous resolution

- [1] a) U. Knof, A. Von Zelewsky, *Angew. Chem.* **1999**, *111*, 312–333; *Angew. Chem. Int. Ed.* **1999**, *38*, 302–322; b) H. Amouri, M. Gruselle, *Chirality in Transition Metal Chemistry: Molecules, Supramolecular Assemblies and Materials*, Wiley, Chichester, **2008**; c) J. Crassous, *Chem. Soc. Rev.* **2009**, *38*, 830–845; d) J. Crassous, *Chem. Commun.* **2012**, *48*, 9684–9692; e) E. B. Bauer, *Chem. Soc. Rev.* **2012**, *41*, 3153–3167.
- [2] a) G. L. J. A. Rikken, E. Raupach, *Nature* **1997**, *390*, 493–494; b) C. Train, R. Gheorghe, V. Krstic, L. M. Chamoreau, N. Ovanesyan, G. Rikken, M. Gruselle, M. Verdaguer, *Nat. Mater.* **2008**, *7*, 729–734; c) C. Train, M. Gruselle, M. Verdaguer, *Chem. Soc. Rev.* **2011**, *40*, 3297–3312.
- [3] For recent examples on metal complexes of 2-(hydroxymethyl)pyridine, see: a) R. Pattacini, P. Teo, J. Zhang, Y. Lan, A. K. Powell, J. Nehrkorn, O. Waldmann, T. S. A. Hor, P. Braunstein, *Dalton Trans.* **2011**, *40*, 10526; b) T. Taguchi, W. Wernsdorfer, K. A. Abboud, G. Christou, *Inorg. Chem.* **2010**, *49*, 10579; c) M. Hubrich, M. Peukert, W. Seichter, E. Weber, *Polyhedron* **2010**, *29*, 1854; d) S. G. Telfer, N. D. Parker, R. Kuroda, T. Harada, J. Lefebvre, D. B. Leznoff, *Inorg. Chem.* **2008**, *47*, 209; e) V. T. Yilmaz, S. Hamamci, C. Thone, *Polyhedron* **2004**, *23*, 841; f) M. Ito, S. Onaka, *Inorg. Chim. Acta* **2004**, *357*, 1039; for complexes of 3- and/or 4-(hydroxymethyl)pyridine, see: g) N. I. Jakab, Z. Vaskova, J. Moncol, B. Gyurcsik, J. Sima, M. Koman, D. Valigura, *Polyhedron* **2010**, *29*, 2262; h) R. Murugavel, S. Kuppuswamy, N. Gogoi, R. Boomishankar, A. Steiner, *Chem. Eur. J.* **2010**, *16*, 994; i) A. Bacchi, M. Carcelli, T. Chiodo, F. Mezzadri, *CrystEngComm* **2008**, *10*, 1916.
- [4] a) V. Terrasson, Y. García, P. Farràs, F. Teixidor, C. Viñas, J. G. Planas, D. Prim, M. E. Light, M. B. Hursthouse, *CrystEngComm* **2010**, *12*, 4109; b) F. Di Salvo, B. Camargo, Y. García, F. Teixidor, C. Viñas, J. G. Planas, M. E. Light, M. B. Hursthouse, *CrystEngComm* **2011**, *13*, 5788; c) F. Di Salvo, C. Paterakis, M. Y. Tsang, Y. García, C. Viñas, F. Teixidor, J. G. Planas, M. E. Light, M. B. Hursthouse, D. Choquesillo-Lazarte, *Cryst. Growth Des.* **2013**, *13*, 1473–1484.
- [5] a) D. Olid, R. Núñez, C. Viñas, F. Teixidor, *Chem. Soc. Rev.* **2013**, *42*, 3318–3336; b) F. Teixidor, C. Viñas in *Science of Synthesis, Vol. 6*, Thieme, Stuttgart, **2005**, p. 1235, and references therein; c) R. N. Grimes, *Carboranes, 2nd ed.*, Elsevier, Amsterdam, **2011**.
- [6] M. Scholz, E. Hey-Hawkins, *Chem. Rev.* **2011**, *111*, 7035, and references therein.
- [7] a) L. Schwartz, L. Eriksson, R. Lomoth, F. Teixidor, C. Viñas, S. Ott, *Dalton Trans.* **2008**, 2379–2381; b) R. Núñez, P. Farràs, F. Teixidor, C. Viñas, R. Sillanpää, R. Kivekäs, *Angew. Chem.* **2006**, *118*, 1292–1294; *Angew. Chem. Int. Ed.* **2006**, *45*, 1270–1272; c) F. Teixidor, R. Núñez, C. Viñas, R. Sillanpää, R. Kivekäs, *Angew. Chem.* **2000**, *112*, 4460–4462; *Angew. Chem. Int. Ed.* **2000**, *39*, 4290–4292.
- [8] F. Di Salvo, F. Teixidor, C. Viñas, J. G. Planas, M. E. Light, M. B. Hursthouse, N. Aliaga-Alcalde, *Cryst. Growth Des.* **2012**, *12*, 5720.
- [9] a) Y.-Y. Zhu, X. Guo, C. Cui, B.-W. Wang, Z.-M. Wang, S. Gao, *Chem. Commun.* **2011**, *47*, 8049–8051; b) E. C. Constable, G. Zhang, C. E. Housecroft, M. Neuberger, J. A. Zampese, *Chem. Commun.* **2010**, *46*, 3077–3079; c) R. Singh, A. Banerjee, E. Colacio, K. K. Rajak, *Inorg. Chem.* **2009**, *48*, 4753–4762.
- [10] C. Train, T. Nuida, R. Gheorghe, M. Gruselle, S. Ohkoshi, *J. Am. Chem. Soc.* **2009**, *131*, 16838–16843.
- [11] W.-Q. Chen, Y.-M. Chen, T. Lei, W. Liu, Y. Li, *Inorg. Chem. Commun.* **2012**, *19*, 4–9.
- [12] K. Butsch, A. Klein, M. Bauer, *Inorg. Chim. Acta* **2011**, *374*, 350 and references therein.
- [13] E. Y. Tshuva, S. J. Lippard, *Chem. Rev.* **2004**, *104*, 987.
- [14] Y. Zang, Y. Dong, L. Que, Jr., K. Kauffmann, E. Münck, *J. Am. Chem. Soc.* **1995**, *117*, 1169.

- [15] I. Shweky, A. Bino, D. P. Goldberg, S. J. Lippard, *Inorg. Chem.* **1994**, *33*, 5161.
- [16] Mercury: visualization and analysis of crystal structures. C. F. Macrae, P. R. Edgington, P. McCabe, E. Pidcock, G. P. Shields, R. Taylor, M. Towler, J. van de Streek, *J. Appl. Crystallogr.* **2006**, *39*, 453–457.
- [17] For simple hmpH structures, see: a) J.-P. Sun, L.-C. Li, X.-J. Zheng, *Inorg. Chem. Commun.* **2011**, *14*, 877–881; b) VOJTAQ, VOJTEU: T. Taguchi, T. C. Stamatatos, K. A. Abboud, C. M. Jones, K. M. Poole, T. A. O'Brien, G. Christou, *Inorg. Chem.* **2008**, *47*, 4095–4108; c) YAZDUY: C. A. Christmas, H.-L. Tsai, L. Pardi, J. M. Kesselman, P. K. Gantzel, R. K. Chadha, D. Gatteschi, D. F. Harvey, D. N. Hendrickson, *J. Am. Chem. Soc.* **1993**, *115*, 12483–12490.
- [18] The average Fe–O bond length (18 bonds) for the four structures for **1** given in this paper is 2.069 Å. The corresponding average for phenyl derivative **3** (8 bonds) is 1.982 Å and that for the 2-methoxyphenyl-hmpH (4 bonds) is 1.971 Å (ETISUW in ref. [12]).
- [19] Note that the sign given refers here to the specific rotation at $\lambda = 589$ nm in dichloromethane. Indeed, opposite signs have been observed in CD spectra of **oCBhmpH** in dichloromethane between $\lambda = 230$ and 260 nm and in HPLC conditions (hexane/EtOH 80:20) with a CD detector at $\lambda = 254$ nm. The specific rotations in dichloromethane also change sign from (S)-(–)-**oCBhmpH** to (SSR)-(+)–**1**.
- [20] F. Delbecq, P. Sautet, *J. Am. Chem. Soc.* **1992**, *114*, 2446–2455.
- [21] H. E. Smith in *Circular Dichroism: Principles and Applications*, 2nd ed., (Eds.: N. Berova, K. Nakanishi, R. W. Woody), Wiley-VCH, Weinheim, **2000**.
- [22] H. D. Flack, *Acta Crystallogr. Sect. A* **1983**, *39*, 876.
- [23] a) J. Jacques, A. Collet, S. H. Wilen, *Enantiomers, Racemates, and Resolutions*, Krieger, Malabar, **1994**; b) G. Coquerel, *Novel Optical Resolution Technologies*, Springer, Berlin, Heidelberg, **2007**, p. 1; c) L. Pérez-García, D. B. Amabilino, *Chem. Soc. Rev.* **2007**, *36*, 941–967.
- [24] a) P. S. Halasyamani, K. R. Poeppelmeier, *Chem. Mater.* **1998**, *10*, 2753–2769; b) K. M. Ok, E. O. Chi, P. S. Halasyamani, *Chem. Soc. Rev.* **2006**, *35*, 710–717.
- [25] Y. Amharar, S. Petit, M. Sanselme, Y. Cartigny, M.-N. Petit, G. Coquerel, *Cryst. Growth Des.* **2011**, *11*, 2453–2462.
- [26] a) K. Kinbara, Y. Hashimoto, M. Sukegawa, H. Nohira, K. Saigo, *J. Am. Chem. Soc.* **1996**, *118*, 3441–3449; b) A. Galland, V. Dupray, B. Berton, S. Morin, M. Sanselme, H. Atmani, G. Coquerel, *Cryst. Growth Des.* **2009**, *9*, 2713–2718.
- [27] O. Kahn, *Molecular Magnetism*, Wiley-VCH, New York, **1993**, pp. 23–26.
- [28] A. Doudouh, C. Woltermann, P. C. Gos, *J. Org. Chem.* **2007**, *72*, 4978.
- [29] COLLECT data collection software, B. V. Nonius, **1998**.
- [30] Z. Otwinowski, W. Minor, *Methods in Enzymology*, Vol. 276: Processing of X-ray Diffraction Data Collected in Oscillation Mode of Macromolecular Crystallography, Part A (Eds.: C. W. Carter, Jr., R. M. Sweet), Academic Press, New York, **1997**, pp. 307–326.
- [31] G. M. Sheldrick, SADABS, Bruker Nonius area-detector scaling and absorption correction, V2.10.
- [32] CrystalClear-SM Expert 2.0 r7 (Rigaku, 2011).
- [33] G. M. Sheldrick, SHELX97, Programs for Crystal Structure Analysis (Release 97-2), University of Göttingen, Göttingen, Germany, **1998**.
- [34] J. Bruno, J. C. Cole, P. R. Edgington, M. Kessler, C. F. Macrae, P. McCabe, J. Pearson, R. Taylor, *Acta Crystallogr. Sect. B* **2002**, *B58*, 389.
- [35] CrysAlis CCD and CrysAlis RED, versions 1.171.33.55; Oxford Diffraction Ltd: Yarnton, Oxfordshire, UK, **2012**.
- [36] O. V. Dolomanov, A. J. Blake, N. R. Champness, M. J. Schröder, *Appl. Crystallogr.* **2003**, *36*, 1283.
- [37] G. M. Sheldrick, SHELXS-97 and SHELXL-97; University of Göttingen: Göttingen, Germany, **1997**.
- [38] Bruker, APEX2 Software, Bruker AXS Inc. V2012.2, Madison, Wisconsin, USA, **2012**.
- [39] Bruker, SAINT, Area Detector Integration Software, Bruker AXS Inc., V8.18c Madison, Wisconsin, USA, **1997**.
- [40] SQUEEZE: P. van der Sluis, A. L. Spek, *Acta Crystallogr. Sect. A* **1990**, *46*, 194–201.
- [41] S. Clevers, F. Simon, V. Dupray, G. Coquerel, *J. Therm. Anal. Calorim.* **2013**, *112*, 271–277.
- [42] For a powder technique for the evaluation of nonlinear optical materials, see: S. K. Kurtz, T. T. Perry, *J. Appl. Phys.* **1968**, *39*, 3798–3813.
- [43] a) E. Ruiz, P. Alemany, S. Alvarez, J. Cano, *J. Am. Chem. Soc.* **1997**, *119*, 1297–1303; b) E. Ruiz, J. Cano, S. Alvarez, *Chem. Eur. J.* **2005**, *11*, 4767–4771; c) E. Ruiz, T. Cauchy, J. Cano, R. Costa, J. Tercero, S. Alvarez, *J. Am. Chem. Soc.* **2008**, *130*, 7420–7426.
- [44] a) E. Ruiz, *Struct. Bonding* **2004**, *113*, 71–102; b) E. Ruiz, S. Alvarez, J. Cano, V. Polo, *J. Chem. Phys.* **2005**, *123*, 164110.
- [45] E. Ruiz, J. Cano, S. Alvarez, P. Alemany, *J. Comp. Chem.* **1999**, *20*, 1391–1400.
- [46] E. Ruiz, A. Rodríguez-Forteza, J. Cano, S. Alvarez, P. Alemany, *J. Comp. Chem.* **2003**, *24*, 982–989.
- [47] E. Ruiz, A. Rodríguez-Forteza, J. Tercero, T. Cauchy, C. Massobrio, *J. Chem. Phys.* **2005**, *123*, 074102.
- [48] A. D. Becke, *J. Chem. Phys.* **1993**, *98*, 5648–5652.
- [49] A. Schäfer, C. Huber, R. Ahlrichs, *J. Chem. Phys.* **1994**, *100*, 5829–5835.
- [50] Gaussian 09, Revision B.01, M. J. Frisch, G. W. Trucks, H. B. Schlegel, G. E. Scuseria, M. A. Robb, J. R. Cheeseman, G. Scalmani, V. Barone, B. Menucci, G. A. Petersson, H. Nakatsuji, M. Caricato, X. Li, H. P. Hratchian, A. F. Izmaylov, J. Bloino, G. Zheng, J. L. Sonnenberg, M. Hada, M. Ehara, K. Toyota, R. Fukuda, J. Hasegawa, M. Ishida, T. Nakajima, Y. Honda, O. Kitao, H. Nakai, T. Vreven, J. A. Montgomery, Jr., J. E. Peralta, F. Ogliaro, M. Bearpark, J. J. Heyd, E. Brothers, K. N. Kudin, V. N. Staroverov, R. Kobayashi, J. Normand, K. Raghavachari, A. Rendell, J. C. Burant, S. S. Iyengar, J. Tomasi, M. Cossi, N. Rega, J. M. Millam, M. Klene, J. E. Knox, J. B. Cross, V. Bakken, C. Adamo, J. Jaramillo, R. Gomperts, R. E. Stratmann, O. Yazyev, A. J. Austin, R. Cammi, C. Pomelli, J. W. Ochterski, R. L. Martin, K. Morokuma, V. G. Zakrzewski, G. A. Voth, P. Salvador, J. J. Dannenberg, S. Dapprich, A. D. Daniels, Ö. Farkas, J. B. Foresman, J. V. Ortiz, J. Cioslowski, D. J. Fox, Gaussian, Inc., Wallingford CT, **2009**.
- [51] *Jaguar 7.0*: Schrödinger, LLC, New York, **2007**.
- [52] G. Vacek, J. K. Perry, J.-M. Langlois, *Chem. Phys. Lett.* **1999**, *310*, 189–194.

Received: August 2, 2013

Published online on December 12, 2013